Domain wall and interphase boundary motion in a two-phase morphotropic phase boundary ferroelectric: Frequency dispersion and contribution to piezoelectric and dielectric properties

Jacob L. Jones, Elena Aksel, Goknur Tutuncu, Tedi-Marie Usher, Jun Chen, Xianran Xing, and Andrew J. Studer

Phys. Rev. B **86**, 024104 — Published 12 July 2012

DOI: 10.1103/PhysRevB.86.024104

Domain wall and interphase boundary motion in a two-phase morphotropic phase boundary ferroelectric: frequency dispersion and contribution to piezoelectric and dielectric properties

Jacob L. Jones[1,2*] , Elena Aksel,[1] Goknur Tutuncu,[1] Tedi-Marie Usher,[1] Jun Chen,[3] Xianran Xing,[3] and Andrew J. Studer[4]

[1]*Department of Materials Science and Engineering, University of Florida, Gainesville, FL 32611, USA*

[2]*School of Materials Science and Engineering, University of New South Wales, NSW 2052, Australia*

[3]*Department of Physical Chemistry, University of Science and Technology Beijing, Beijing 100083, China*

[4]*Bragg Institute, Australian Nuclear Science and Technology Organisation, Lucas Heights, Australia*

[*] Corresponding Author: email jjones@mse.ufl.edu, telephone 352-846-3788

In ferroelectric materials, enhanced dielectric and piezoelectric property coefficients are found in compositions near morphotropic phase boundaries (MPBs). The material response in these compositions may be contributed by enhanced intrinsic piezoelectric distortions or increased interface motion, *e.g.* contributions from domain wall and interphase boundary motion, though the relative effect of these mechanisms in different materials is not yet well understood. One of the major challenges to developing this understanding is the availability and sensitivity of *in situ* characterization techniques, particularly during the application of cyclic electric fields of subcoercive or weak amplitude, conditions at which the property coefficients are measured. Here, we use time-resolved neutron diffraction to resolve the subtle electric-field-induced crystallographic strain mechanisms in a prototypical MPB composition, 36%$BiScO_3$-64%$PbTiO_3$, that contains coexisting monoclinic and tetragonal phases. We observe multiple cooperative electromechanical effects including domain wall motion in both the monoclinic and tetragonal phases, interphase boundary motion between the two phases, and electric-field-induced lattice strains. The measured effects span four orders of magnitude in frequency, facilitating the discrimination of intrinsic and extrinsic contributions to properties. Domain wall motion in the monoclinic phase dominates the response, leading to shifts of diffraction peaks as high as 2300 pm/V; these shifts reflect the field-induced changes in average pseudo-cubic (00*h*) lattice spacing of the monoclinic phase parallel to the electric field. Domain wall motion in the tetragonal phase is also readily apparent and exhibits a degree of frequency dispersion similar to that measured in both the relative permittivity and piezoelectric coefficients at similar conditions.

I. INTRODUCTION

The dielectric, piezoelectric, and electromechanical coupling properties of ferroelectric materials are often enhanced near phase boundaries.[1-3] This behavior can be explained by several different intrinsic and extrinsic effects which, in some cases, may combine or work cooperatively to enable a large response.[4] For example, enhanced intrinsic contributions have been attributed to higher dielectric, piezoelectric, and elastic susceptibility approaching phase transitions.[5-7] Extrinsic contributions such as increased domain wall motion or domain switching has been observed or suggested at compositions on[8] or near[4] the phase boundaries. The presence of monoclinic[9] or nanodomain[10] structures have also been suggested to enhance the properties by flattening of the free energy profile (intrinsic)[11] or by enabling greater domain wall contributions (extrinsic).[12] However, the effect of these phenomena on property enhancement is not yet clear as monoclinic phases[13] and nanodomains[14] have been observed in other materials which do not exhibit enhanced properties.

The contribution of interface displacement (*e.g.*, domain wall motion) to the dielectric and piezoelectric coefficients can been quantified in some cases by evaluating the field-amplitude or frequency-dependence of the property coefficients. For example, a linear field-amplitude dependence of dielectric permittivity is often observed at electric field amplitudes below the coercive field (E_c) and may suggest the presence of such extrinsic contributions.[15] This behavior is described phenomenologically using the Rayleigh law, which implies a random distribution of pinning centers interacting with the displacing interface.[15]

Frequency dispersion in polycrystalline ferroelectric materials is not understood as well, but can also be used to assess the extent of extrinsic contributions. Frequency dispersion in dielectric permittivity due to domain wall displacement is often considered to occur at frequencies near 10^9 Hz.[15] At frequencies as low as 1 Hz, however, many ferroelectric materials exhibit dispersion in

the elastic,[16,17] dielectric,[18,19] and piezoelectric[20] coefficients. From 0.01 Hz to 100 Hz, for example, Damjanovic *et al.* observed a decrease of approximately 10% in the longitudinal piezoelectric coefficient of a lead zirconate titanate (PZT) composition and a decrease of 50% in a Sm-modified $PbTiO_3$ composition.[21] The extent of frequency dispersion is one method of separating the intrinsic and extrinsic contributions to the properties; *i.e.*, extrinsic contributions can be frequency dependent while the intrinsic piezoelectric effect can be frequency independent.[15,22]

The contribution of interface displacement to the property coefficients can also be observed and quantified using X-ray and neutron diffraction, where domain wall displacement or motion is measured as a change in volume or phase fraction of different ferroelastic phases or orientation variants. Using this approach, the contribution of domain wall motion to the piezoelectric coefficient has been characterized in compositions containing a single ferroelectric phase.[4,23] In certain compositions of these materials, domain wall motion has been shown to directly account for more than half of the electric-field-induced strain at weak to intermediate field amplitudes.[4,23]

In single-phase compositions near phase boundaries, nonlinear effects in the macroscopic strain and polarization can also result from electric-field-induced phase transitions during application of high electric field amplitudes. This has been observed in both polycrystalline (*e.g.*, Refs. 1,24) and single crystalline materials (*e.g.*, Refs. 25,26). Certain compositions closer to phase boundaries have been shown to exhibit two or more phases in coexistence.[27-29] In such cases, it has been suggested that the motion of the interface separating these phases, or interphase boundary motion, may significantly affect the macroscopic properties[1,29-31] such as dielectric and piezoelectric coefficients. During application of stepwise static electric fields of high amplitude (greater than E_c), large-scale nonlinearities in phase fractions have been observed using X-ray and neutron diffraction, *e.g.* as in Ref. 28. However, direct measurement of interphase boundary

motion at weak to intermediate field amplitudes, conditions at which property coefficients are measured, has eluded researchers.[1,31] This type of interface motion, if measured directly, is important for understanding the dielectric, piezoelectric, and electromechanical coupling properties of compositions containing multiple phases or near phase boundaries. In order to measure this interface motion directly, *in situ* characterization probes are needed which are capable of measuring subtle boundary motion during application of subcoercive, cyclic electric fields. Such probes may concurrently characterize other contributions to the electromechanical or piezoelectric coupling.

In the present work, we use the high speed neutron diffractometer Wombat at the Australian Nuclear Science and Technology Organisation (ANSTO)[32] to confirm and measure the extent of interphase boundary and domain wall motion in a two-phase morphotropic phase boundary (MPB) ferroelectric during application of cyclic electric fields of subcoercive or weak-field amplitude. Wombat operates in an angularly dispersive open geometry with a monochromatic beam. The instrument uses a high speed detector[33,34] that timestamps all neutron events; time-resolved data is acquired stroboscopically and is synchronized with the cyclic electric field. The sub-millisecond timing accuracy is defined only by time-of-flight dispersion of the neutrons from the sample to the detector. This is comparable to the time response of the detector itself, meaning that the maximum timing resolution has been achieved for such instrumentation at a reactor source.

These measurements are demonstrated on a polycrystalline ferroelectric composition in the solid solution (1-x)$BiScO_3$-x$PbTiO_3$ (BS-100xPT). The studied composition is near the MPB at x=0.64[35] and contains coexisting monoclinic and tetragonal phases. Longitudinal piezoelectric coefficients of this composition have been reported near 500 pC/N (or pm/V),[36] implying that large crystallographic changes may expected. Moreover, mechanisms of electromechanical strain

in Bi-based[29,37-39] and Pb-based[9,10,28,40] perovskites are under intense present investigation and phase boundaries between these two unique components provide scientific insight that is relevant to a wide variety of dielectric materials.

II. EXPERIMENTAL

Samples of BS-64PT were prepared by solid-state reaction of PbO, TiO_2, Bi_2O_3, and Sc_2O_3. Stoichiometric mixtures were ball milled in ethanol for 12 h, dried, calcined at 760 °C for 5 h, and ball milled for an additional 12 h. Powders were then uniaxially pressed into bar-shaped dies and then sintered in a covered crucible at 1100 °C for 1 h. Laboratory X-ray diffraction of the synthesized polycrystalline materials confirmed the coexistence of a tetragonal phase with another polymorph, consistent with prior observations of coexistence of the tetragonal phase with a rhombohedral[41] or monoclinic[29] phase.

Disc-shaped samples of 0.75 mm thickness and 8.7 mm diameter were used for property coefficient characterization. Polarization and strain were measured using a Ferroelectricity Analyzer (TF1000, aixACCT, Germany). Polarization and strain were measured at field amplitudes above the coercive field on initially unpoled materials using triangular waveforms and a frequency of 10 Hz. Electrical poling of unpoled samples was completed at a temperature of 100°C using a constant electric field of 4 kV/mm for 10 min. The direct longitudinal piezoelectric coefficient was measured on multiple locations of multiple samples using a Berlincourt d_{33} meter (ZJ-6A, CAS), for which the average and standard deviation (σ) are reported. Polarization and strain were again measured using bipolar electric fields with amplitudes of ±750 V/mm (below the coercive field, or subcoercive) and frequencies varying between 0.01 Hz and 10 Hz.

For the neutron diffraction measurements, gold electrodes were sputter coated on the 3.9 mm × 22.94 mm faces of a 4.1 mm thick sample and overcoated with conducting silver paste. The sample was immersed in fluorinert dielectric fluid inside a Kapton tube and electrical leads were connected to a Trek 2000:1 high voltage amplifier (model 20/20) driven by an Agilent arbitrary waveform generator and synchronized with the Wombat diffractometer. The Wombat detector spans a diffraction angle of 120° at a radius of 700 mm. A constant wavelength of 2.95 Å was used for all measurements. The sample was mounted with the electric field direction between the scattering vectors for the {002} and {111} profiles. The angle between the electric field and the scattering vectors of planes being measured is given by $\varphi=(90°-2\theta)/2$. The {111} and {002} reported in the present work are therefore $\varphi=5.5°$ and $\varphi=2.2°$, respectively. In polycrystalline ferroelectric materials, planes at these angles to the field direction behave similarly to those at $\varphi=0°$.[4,42] Thus, the presented diffraction patterns describe a sample response that is nearly equivalent to that measured perfectly parallel to the electric field direction.

III. RESULTS

A. Ferroelectric, Dielectric, and Piezoelectric Properties

The dielectric and piezoelectric properties of the samples were initially characterized as a function of field amplitude and frequency. Some of the field-amplitude-dependent results are reported in Ref. 43. Similar measurements in the present work are completed using field amplitudes less than half of the coercive field ($< 0.5E_c$).

The direct longitudinal piezoelectric coefficient, d_{33}, is described by the equation

$$D_3 = d_{33}T_3, \quad (1)$$

where D_3 is the dielectric displacement parallel to the poling direction, measured in response to a longitudinal stress T_3 applied parallel to the poling direction. The direct piezoelectric coefficient for samples synthesized in the present work is d_{33} = 461 pC/N (σ = 11 pC/N). Within error, this is equal to the values of 460 pC/N reported previously by Eitel *et al.*[35]

The polarization and strain of this composition in response to a bipolar electric field with amplitude greater than E_c are shown in Fig. 1. The remanent polarization after positive and negative electric field application is P_r = 44 μC/cm^2. The coercive field, E_c, is defined in the present work as the electric field amplitude at which the polarization becomes zero. This value is 2.2 kV/mm in both positive and negative electric field directions. The peak-to-peak strain is 0.58% under a ±5 kV/mm bipolar electric field.

After poling, the samples were subjected to cyclic electric fields of amplitude ±750 V/mm (or subcoercive at 0.34E_c). Two representative polarization and strain measurements are shown in Figs. 2(a) and 2(b). These representative measurements demonstrate a decrease in the peak-to-peak polarization and strain with increasing frequency. Lower frequencies (*i.e.*, 0.1 Hz) generate a larger material response and higher frequencies (*i.e.*, 10 Hz) generate a smaller response. The average polarization and strain response was fit to a line in order to further characterize the pseudo-linear property coefficients. The change in polarization (equivalent to dielectric displacement at these subcoercive amplitudes) can be related to the dielectric permittivity through the equation

$$D_3 = \varepsilon_{r,33}\varepsilon_o E_3 , \tag{2}$$

where E_3 is the electric field amplitude, ε_o is the permittivity of free space (8.854·10^{-12} F/m), and $\varepsilon_{r,33}$ is the relative permittivity of the material (hereafter simplified to ε_r). The longitudinal strain response to the electric field is related to the longitudinal converse piezoelectric coefficient, d_{33}.

This coefficient is theoretically equivalent to the direct piezoelectric coefficient and is described by the equation

$$S_3 = d_{33}E_3, \quad (2)$$

where S_3 is the mechanical strain parallel to the poling direction.

The values for the dielectric and converse piezoelectric coefficients, ε_r and d_{33}, are shown in Fig. 2(c) as a function of frequency. The coefficients measured at 1 Hz are ε_r = 3230 and d_{33} = 660 pm/V, similar to the values reported previously by Eitel *et al.* under similar loading conditions.[44] Moreover, one of the most defining features of the results in Fig. 2(c) is the frequency dependence of the property coefficients: a decrease of 26% in ε_r and 21% in d_{33} is observed across four order of magnitude in frequency.

B. In Situ Neutron Diffraction Measurements: Quasi-static Electric Fields

To measure the crystallographic changes during the application of electric fields to an initially unpoled material, constant electric field amplitudes were applied in steps of 0.5 kV/mm to a maximum of +3.0 kV/mm and diffraction patterns were measured for 10 minutes at each electric field step. Diffraction profiles near the pseudo-cubic (PC) $\{002\}_{PC}$ and $\{111\}_{PC}$ reflections are shown in Figs. 3(a) and 3(b), respectively.

Significant changes in the $\{002\}_{PC}$ diffraction patterns are observed at 1.5 kV/mm. Some of these changes involve redistribution of component peak intensities of ferroelastic degenerate peaks, an effect attributed to domain switching during the electrical poling process.[42] The $\{002\}_{PC}$ profile contains at least three obvious Bragg peaks; the tetragonal $(002)_T$ and $(200)_T$ reflections are observed at the lowest and highest 2θ positions, respectively, and additional Bragg scattering is observed between these two reflections. This additional Bragg scattering may

be interpreted as the $(002)_R$ reflection of a rhombohedral phase[41] or, more recently, has been associated with the $(002)_M$ and $(220)_M$ reflections of a monoclinic phase (space group *Cm*).[29] Using the refined crystallographic data for the monoclinic phase of BS-64PT from Kim *et al.*,[29] the $(002)_M$ and $(220)_M$ interplanar spacings can be shown to differ by 0.78%. Their corresponding reflections are not separately resolved in the present measurement due to the broad diffuse scattering observed in ferroelastic materials[45] and partial overlap with the shoulders of the tetragonal phase reflections [Fig. 3(c)]. These additional reflections are therefore fit in the present work using a single profile and referenced relative to the pseudo-cubic (PC) perovskite unit cell as $\{002\}_{PC,M}$.

The contributing reflections to the $\{111\}_{PC}$ profile [Fig. 3(b)] are not measurably split and an asymmetric profile shape function is observed in the initial unpoled state. At 1.5 kV/mm, this profile shifts dramatically to lower 2θ. By fitting this diffraction profile to a Gaussian profile shape function, the peak shift can be shown to correspond to a change in the average {111} interplanar spacing from 2.309 Å to 2.321 Å, or a strain of 0.54%. While the tetragonal phase has a single (111) reflection, the monoclinic phase has two contributing Bragg reflections to this profile, the $(201)_M$ and $(021)_M$. Changing intensities between these Bragg reflections, a signature in diffraction of ferroelastic domain wall motion,[42] would be observed in this broad $\{111\}_{PC,M}$ diffraction profile as a peak shift during electric field application. This large strain of 0.54% may therefore be contributed significantly by ferroelastic domain wall motion in the monoclinic phase.

C. In Situ Neutron Diffraction Measurements: Cyclic, Subcoercive Fields

After electrical poling, the samples were allowed to age for 48 hours to mitigate the potential effects of initial ageing on ferroelectric behavior.[46] The samples were then subjected to cyclic,

bipolar square wave electric fields of amplitude ±750 V/mm. The use of a square wave for these measurements provides the specific advantages of: 1) if relaxation is present in the material response, a square wave enables the measurement of this relaxation directly; 2) if relaxation effects are not apparent, then all diffracted intensities that are measured during each respective electric field state may be summed in order to increase the total measurement counts.[23] Moreover, there have been negligible differences reported between the material responses of ferroelectric materials under application of subcoercive square and sine waves.[4] The amplitude applied in the present work is 34% of E_c and is in the region where Rayleigh behavior (*i.e.*, linear field-amplitude dependence of ε_r and d_{33}) has been observed in the dielectric and piezoelectric coefficients of this composition.[43,44] The measurements were completed across four orders of magnitude of frequency in the following order: 1 Hz, 10 Hz, 0.01 Hz, and 0.1 Hz. The frequencies were intentionally non-sequential such that any effects of fatigue or deaging[43] could be identified from an authentic frequency dependence of the coefficients.

The response of the sample at each frequency was measured for 120 minutes continuously. Measured neutrons were time stamped in stroboscopic mode using 128 time bins within each cycle (*e.g.*, ~8 ms time periods for the 1 Hz frequency). A time-dependent relaxation was not evident in the time-resolved diffraction pattern at any of the frequencies and the data was therefore reduced to 2 time bins corresponding to the two polarities of the bipolar waveform. Representative $\{002\}_{PC}$ and $\{111\}_{PC}$ diffraction profiles corresponding to the two polarities of the 1 Hz waveform are shown in Figs. 3(c) and 3(d). The $\{111\}_{PC}$ peak [Fig. 3(d)] shows an average shift to lower 2θ during the positive polarity. In the $\{002\}_{PC}$ reflections [Fig. 3(c)], domain wall motion is observed in the tetragonal phase by an increase in the intensity of the $(002)_T$ tetragonal phase reflection and a corresponding decrease in the intensity of the $(200)_T$

tetragonal phase reflection. The monoclinic $\{002\}_{PC,M}$ profile is also observed to shift to a lower 2θ position.

The {002} diffraction profiles were fit to three Gaussian profile shape functions to extract integrated intensity and position of the tetragonal $(002)_T$ and $(200)_T$ and monoclinic $\{002\}_{PC,M}$ components. Domain wall motion in the tetragonal phase is expressed by the ratio of the $(002)_T$ to $(200)_T$ peak intensities in Fig. 4(a). It can be seen that the ratio is consistently higher for positive polarity relative to negative polarity, indicating an increase in the volume fraction of domains oriented with their c-axes parallel to the electric field during the positive polarity. During negative polarity, the volume fraction of domains with their c-axes oriented parallel to the field decreases. This is consistent with the domain wall motion behavior observed previously in single-phase tetragonal lead zirconate titanate (PZT) based materials.[4] The difference between the values measured under positive and negative polarities, shown at the bottom of Fig. 4(a), demonstrates a statistically significant difference within a 68% confidence interval extracted from the profile fit [Fig. 4(a)]. Within a 95% confidence interval, measurable differences are apparent in the data measured at the three lowest frequencies of 0.01 Hz, 0.1 Hz, and 1 Hz. These nonzero differences in the intensity ratios indicate that domain walls are moving in the tetragonal phase of the material during application of the cyclic, subcoercive electric fields.

To describe the relative volume fractions of the monoclinic and tetragonal phases, the ratio of the monoclinic $\{002\}_{PC,M}$ intensity to the total tetragonal {002} intensity [*i.e.*, the sum of $(002)_T$ and $(200)_T$ integrated intensities] is introduced. These results are shown in Fig. 4(b) and demonstrate a small but clearly distinguishable change in the value between positive and negative polarity. The change in this value indicates a change in the monoclinic to tetragonal phase fraction between positive and negative polarity. The monoclinic phase fraction is consistently larger during positive polarity than negative polarity, evidence of weak but

measurable interphase boundary motion during application of subcoercive, cyclic electric fields. This observation is clear for all frequencies within the 68% confidence interval. Within a 95% confidence interval, a significant difference is also measurable between positive and negative polarity at the three lowest frequencies of 0.01 Hz, 0.1 Hz, and 1 Hz. Because a change in phase fraction necessitates the motion of boundaries separating these phases, the present work demonstrates small but measurable interphase boundary motion between coexisting tetragonal and monoclinic phases.

Electric-field-induced lattice strains (ε_{hkl}) are calculated from the shift in diffraction profiles between the positive and negative electric field polarities. The respective strain coefficients ($d_{hkl}=\varepsilon_{hkl}/E$) are shown in Fig. 5 as a function of frequency. For the tetragonal $(002)_T$ and $(200)_T$ peaks, the strain coefficients represent the electric-field-induced lattice strain coefficient of the respective planes. For the monoclinic phase, the single $\{002\}_{PC,M}$ profile is constituted of two contributing reflections. Therefore, the strain coefficient for this peak represents the average displacement or strain of the pseudo-cubic {002} planes of the monoclinic phase. The mechanism for straining in this monoclinic phase could be lattice strains (*i.e.*, near-continuous change in spacing with force amplitude) or could be the result of interchanging of the contributing ferroelastic degenerate planes (*i.e.*, domain wall motion).

In single-domain single crystals, strain coefficients can more easily be attributed to intrinsic piezoelectric strain.[47,48] In polycrystalline materials, a complex interaction between domain switching and elastic lattice strain in strain-coupled crystalline orientations has been shown to significantly modify the electric-field-induced strain coefficients.[4,49] For the present ferroelectric polycrystalline materials, Fig. 5 shows that the c-axis lattice parameter of the tetragonal phase [measured in the $(002)_T$ strain coefficient] elongates parallel to the electric field with a strain coefficient greater than 500 pm/V. In contrast, the a-axis lattice parameter [measured in the

$(200)_T$ strain coefficient] does not elongate parallel to the electric field. The $\{002\}_{PC,M}$ profile of the monoclinic phase demonstrates a significantly larger average strain or peak shift than the tetragonal phase {002} reflections with values of approximately 2300 pm/V at frequencies < 0.1 Hz. The other defining feature of the electric-field-induced strain coefficient of the monoclinic profile, $\{002\}_{PC,M}$, is the strong frequency dispersion which reduces the value by 600 pm/V across four orders of magnitude in frequency. This change is equivalent to a reduction in 26% across this frequency range and correlates with the percentage decrease measured in the dielectric permittivity and piezoelectric coefficients at equivalent frequencies and field amplitudes [Fig. 2(c)].

IV. DISCUSSION

It has previously been shown that the pinning of internal interfaces by defects can result in a logarithmic frequency dependence of the piezoelectric coefficients.[20] These internal interfaces may include ferroelectric/ferroelastic domain walls and interphase boundaries. This logarithmic dependence has been observed for two different types of interface displacement including domain wall motion between pinning centers (reversible displacement) and domain wall motion that overcomes pinning centers (irreversible displacement). In the present work, frequency dependence due to domain wall displacement in the tetragonal phase is characterized by measuring the ratio of the $(002)_T$ and $(200)_T$ peak intensities during positive and negative polarity [top of Fig. 4(a)] and their difference [bottom of Fig. 4(a)]. In Fig. 4(a), a frequency dependence is observed in the difference between the tetragonal peak intensities [bottom of Fig. 4(a)], which is shown to decrease monotonically with increased frequency. Because the difference between these values indicates the fraction of domains that are reoriented between the maximum and minimum field amplitudes, this measurement supports domain wall motion in the

tetragonal phase as one origin of the frequency dispersion of property coefficients shown in Fig. 2(c). Specifically, the values decrease from 0.20 at 0.01 Hz to 0.11 at 10 Hz, a decrease of 45% across four orders of magnitude. This percentage decrease is expectedly greater than that observed in the macroscopic property coefficients (*i.e.*, 21%-26%) because the property coefficients contain an additional intrinsic component (dominantly frequency independent) that adds to the measured coefficients. The addition of this component suppresses the degree of frequency dependence due to extrinsic effects such as domain wall motion. Moreover, both reversible and irreversible domain wall motion can exhibit frequency dispersion.[20] Since the present experimental measurements observe both types of domain wall motion, a strong frequency dependence in this behavior is expected.

As the measurements were acquired in the order 1 Hz, 10 Hz, 0.01 Hz, 0.1 Hz, the results in Fig. 4(a) suggest some effect of the measurement order on the results. Specifically, the values of intensity ratio [top of Fig. 4(a)] for 1 Hz and 10 Hz may be artificially higher due to their earlier measurement relative to the measurements at 0.01 Hz and 0.1 Hz. In these same materials, we have reported[43] domain wall motion as the origin of a deaging effect, or an irreversible change (within the timeframe of the experiment) in property coefficients due to application of small alternating fields.[43,50,51] When measuring properties as a function of field amplitude, this effect was shown to change the absolute amount of the oriented domains during the measurement. In other words, a drift in the degree of domain alignment was observed in the backwards direction, towards the unpoled state, with each incremental measurement. However, the difference in the domain alignment between the maximum and minimum field states still obeyed expected trends in field amplitude.[43] The results observed in the present work are equally described by such a deaging effect - influence of the measurement sequence is apparent in the absolute values of intensity [top of Fig. 4(a)] while the difference between the intensity ratio of the different

polarities shows a clear trend with frequency [bottom of Fig. 4(a)]. Thus, deaging seems to affect the absolute domain alignment in the present measurements, though the difference between the domain alignment in the positive and negative polarities still exhibits the expected frequency dispersion.

Interphase boundary motion during subcoercive field application is reported in Fig. 4(b). At each frequency, the ratio of the monoclinic $\{002\}_{PC,M}$ intensity to the total tetragonal {002} intensity is larger during the positive polarity of the waveform than during the negative polarity of the waveform. The results measured at each frequency therefore indicate measurable interphase boundary motion between coexisting tetragonal and monoclinic phases. Although interphase boundary motion has been hypothesized to occur at subcoercive field amplitudes and contribute to dielectric and piezoelectric coefficients,[1,29-31] the present work provides direct evidence of this effect using *in situ*, time-resolved neutron diffraction during electric field application. This type of interface motion is important for understanding the property coefficients of compositions near phase boundaries or containing multiple coexisting phases, e.g. as in Refs. 27-29. The extent of interphase boundary motion measured in the present work [Fig. 4(b)] is not as clearly frequency dependent as domain wall motion in the tetragonal phase [Fig. 4(a)]: the extent of interphase boundary motion decreases from 0.01 to 0.1 Hz and again from 1 to 10 Hz, separated by a discontinuous increase. These results also show some dependence on the measurement sequence (1 Hz, 10 Hz, 0.01 Hz, 0.1 Hz), indicating that a deaging effect may be convoluted in this result with an authentic frequency dependence of the material behavior. The results therefore suggest that interphase boundary motion may be equally or more susceptible to deaging than domain wall motion. Moreover, the interphase boundary motion effects are measurably small relative to domain wall motion in the tetragonal phase.

The lattice strains shown in Fig. 5 provide more insight into the frequency dependence of intrinsic and extrinsic mechanisms. The intrinsic piezoelectric response of the tetragonal phase shows a frequency-independent response and is characterized by a large (~500 pm/V) strain coefficient parallel to [001] and a small strain coefficient (not measurably deviating from 0 pm/V) parallel to [100]. These results are consistent with that of "extender"-type piezoelectrics, where the crystallographic strain is greatest when the electric field is parallel to the polarization direction and less when perpendicular to the polarization.[52] The strain coefficient of the monoclinic {002} profile is much greater by comparison with values near 2300 pm/V at low frequencies. It is not unexpected that this other phase exhibits a high strain coefficient relative to the tetragonal phase: in the [001] direction of BS-xPT single crystals, a larger piezoelectric coefficient was also observed in compositions on the BS-rich ($x<0.64$) side of the MPB ($x = 0.57$, $d_{33} = 1150$ pC/N)[53] than in the PT-rich (tetragonal) compositions ($x = 0.66$, $d_{33} = 200$ pC/N).[54] The present work confirms that such large differences in strain coefficients are also realized in polycrystalline materials containing two distinct crystal symmetries in coexistence. The dependence of strain coefficient on crystal symmetry is also similar to that observed in lead zirconate titanate (PZT)-based ferroelectric materials: the intrinsic piezoelectric strain coefficient in the $[001]_{PC}$ direction of compositions on the $PbZrO_3$-rich (rhombohedral) side of the MPB is larger than that of compositions on the $PbTiO_3$-rich (tetragonal) side.[55,56]

However, this large strain coefficient cannot be attributed entirely to the intrinsic piezoelectric effect of the crystalline lattice. Because at least 600 pm/V of the effect is dependent upon frequency, this amount (and up to the entire 2300 pm/V) of the value may arise from non-intrinsic effects. One possible contribution to this large strain coefficient is that of elastic interaction with other crystallite orientations due to strain coupling. In polycrystalline tetragonal PZT, it was shown that crystalline orientations with $[001]_{PC}$ parallel to the electric field elongate

due to ferroelastic domain reorientation, elastically inducing a strain in orientations that are not favorably oriented for domain wall motion to elongate the grain (*e.g.*, {111} crystalline orientations).[4] The converse is observed in polycrystalline rhombohedral PZT, where {111} oriented grains elongate due to ferroelastic domain wall motion, inducing elastic strain in {002} crystalline orientations.[49] In monoclinic crystal symmetries, where 12 different ferroelastic degenerate orientations are possible, it is expected that domain reorientation is allowed in all crystalline orientations relative to the field direction.[8] Therefore, in the presently investigated samples that contain a mixture of monoclinic (12 degenerate orientations) and tetragonal (3 degenerate orientations) phases, only very weak intergranular constraints may be expected.

A more likely origin of the high $\{002\}_{PC,M}$ strain coefficients and their frequency dependence is that of domain wall motion in the monoclinic phase. Domain wall motion would result in intensity redistribution between ferroelastic degenerate peaks such as the $(002)_M$ and $(220)_M$ reflections (two reflections contributing to the $\{002\}_{PC,M}$ profile) or the $(201)_M$ and $(021)_M$ reflections (two reflections contributing to the {111} profile). The $(002)_M$ and $(220)_M$ interplanar spacings differ by 0.78% (calculated from the refined crystallographic data for the monoclinic phase of BS-64PT from Kim *et al.*[29]) and their respective reflections are not separately resolved in the present measurement. Therefore, changes in their relative intensities would be observed as an overall shift in the $\{002\}_{PC,M}$ profile. An increase in domain volume fraction of the longer ferroelastic lattice spacing at the expense of the shorter ferroelastic lattice spacing [analogous to an increase in the (002)/(200) intensity ratio in the tetragonal phase] would be observed as a shift of the overall diffraction profile to a lower 2θ position as is observed in the present work. Such an extrinsic effect would be expected to be frequency-dependent, also consistent with the present observations in Fig. 5.

Additional evidence for domain wall motion in the monoclinic phase can be found in the {111} profile. Fig. 6 shows the change in the full width at half maximum (FWHM) of the {111} profile between the positive and negative polarities of the waveform. In addition to affecting the intensities of the $(002)_M$ and $(220)_M$ reflections (contributing to the $\{002\}_{PC,M}$ profile), ferroelastic domain wall motion in the monoclinic phase would also affect the relative intensities of the $(201)_M$ and $(021)_M$ reflections that contribute to the measured pseudo-cubic {111} diffraction profile. The changing intensities of these reflections due to domain wall motion would be observed as a peak shift in the {111} diffraction profile [as observed previously in Figs. 3(b) and 3(d)] and a change in the width of the profile. Fig. 6 shows the change in the width of the {111} profile during positive and negative polarity of the waveform and its dependence on frequency. The difference in the profile width between positive and negative polarities is frequency dependent, evidence of an extrinsic origin to this response.

These results suggest that domain wall motion within the monoclinic phase is a strong contribution to the large electric-field-induced lattice strain of 1650-2300 pm/V measured in the monoclinic phase and thus, by extension, to the electric-field-induced strain and piezoelectric coefficient of BS-64PT. It is one of the most dominant changes in the diffraction pattern during electric field perturbation. As discussed previously, the degree of domain switching should be enhanced in materials containing a sufficient number of polarization and ferroelastic variants,[8] as in the present case of a combination of monoclinic and tetragonal phases. However, a large amount of domain switching has been predicted as equally possible in single-phase monoclinic materials.[8] Thus, the significant domain wall motion effects observed in the present work may be ascribed to the low symmetry of the monoclinic phase itself, not necessarily to its coexistence with a tetragonal phase.

Although domain wall motion in the monoclinic phase of the present composition is significant, it should be reinforced that all monoclinic phase materials do not exhibit enhanced domain wall mobility (e.g., $Na_{0.5}Bi_{0.5}TiO_3$ as shown in Ref. 13). This is because there are additional requirements that must be met in order for significant amounts of domain wall motion to be realized in ferroelastic materials. These requirements include, for example, a distribution of pinning centers that does not prohibitively constrain the mobility of domain walls (e.g., as in donor-modified PZT). Each material system and MPB may therefore exhibit unique characteristics which depend, among other factors, on both the composition and combination of phases. Thus, the time-resolved neutron diffraction technique and approaches applied in the present work to an MPB between $BiScO_3$ and $PbTiO_3$ will also be useful in determining the respective contributions of domain wall, interphase boundary motion, and lattice strain in other existing and emerging MPB compositions such as in PZT,[10,28,57] (1-x)$BiFeO_3$-$PbTiO_3$[38,39] and $Na_{0.5}Bi_{0.5}TiO_3$ in solid solution with $BaTiO_3$[24] or $K_{0.5}Bi_{0.5}TiO_3$[58] as well as compositions near polymorphic phase transition temperatures such as those observed in $Na_{0.5}K_{0.5}NbO_3$-based materials.[1,59,60] Based on the results of the present work, it is expected that strong domain wall motion will be observed in some of these materials if they exhibit a sufficient number of ferroelastic variants such that deformation strain is accommodated and intergranular constraints are limited (e.g., as in poly-phase, monoclinic, or other low symmetry materials), and if the strength of pinning centers permit the motion of the walls.

V. CONCLUSIONS

In summary, the present results demonstrate several cooperative crystallographic and microstructural changes in a two-phase MPB ferroelectric during application of cyclic electric fields of subcoercive or weak-field amplitude. The use of frequency as an independent variable

in the measurements enabled discrimination of different types of contributions including electric-field-induced lattice strains and domain wall motion. Intrinsic contributions to the electromechanical response were independent of frequency while extrinsic contributions were shown to depend upon frequency.

Domain wall motion in the monoclinic phase dominated the measured diffraction response. This effect also exhibited a strong frequency dispersion, as evidenced by the frequency dependence of the electric-field-induced lattice strains of the $\{002\}_{PC,M}$ profile and the FWHM of the {111} profile. These strong domain wall motion effects were ascribed to the presence of a sufficient number of polarization and ferroelastic variants - features that can be replicated in other mixed-phase ferroelastic materials. Domain wall motion was also observed in the tetragonal phase by a change in the relative intensity of the $(002)_T$ and $(200)_T$ reflections during the positive and negative polarities of the waveform and this effect decreased with increasing frequency, correlating with a decrease in permittivity and piezoelectric coefficients across the same frequency range. Electric-field-induced lattice strains in the tetragonal phase were largest parallel to the c-axis crystallographic axis (strain greater than 500 pm/V) and an insignificant response was measured in crystallites with their a-axis parallel to the electric field. These lattice strains were not dependent on frequency, indicating their intrinsic piezoelectric origin. The ratio of the monoclinic phase volume fraction to the tetragonal phase volume fraction was also shown to change with electric field polarity, indicating measurable but weak interphase boundary motion at subcoercive electric field amplitudes.

ACKNOWLEDGMENTS

JJ, TU, and GT acknowledge partial support for this work from the U.S. Department of the Army under W911NF-09-1-0435. JJ and EA acknowledge partial support for this work from the

U.S. National Science Foundation under award number DMR-0746902. TU also acknowledges a travel fellowship through the IMI Program of the National Science Foundation under Award No. DMR-0843934. JC acknowledges financial support from the National Natural Science Foundation of China (Grants 91022016 and 21031005). The Bragg Institute at the Australian Nuclear Science and Technology Organisation (ANSTO) is acknowledged for provision of the neutron diffraction facilities through program proposal number PP911. Helpful discussion with John Daniels is gratefully acknowledged.

REFERENCES

[1] Y. Saito *et al.*, Nature **432**, 84 (2004).
[2] Z. Kutnjak, J. Petzelt, and R. Blinc, Nature **441**, 956 (2006).
[3] R. J. Zeches *et al.*, Science **326**, 977 (2009).
[4] A. Pramanick *et al.*, J. Am. Ceram. Soc. **94**, 293 (2011).
[5] D. Damjanovic *et al.*, Journal of Materials Science **41**, 65 (2006).
[6] A. K. Singh *et al.*, Appl. Phys. Lett. **92**, 022910 (2008).
[7] D. Damjanovic, IEEE Transactions on Ultrasonics Ferroelectrics and Frequency Control **56**, 1574 (2009).
[8] J. Y. Li *et al.*, Nat. Mater. **4**, 776 (2005).
[9] R. Guo *et al.*, Phys. Rev. Lett. **84**, 5423 (2000).
[10] K. A. Schönau *et al.*, Phys. Rev. B **75**, 184117 (2007).
[11] H. X. Fu, and R. E. Cohen, Nature **403**, 281 (2000).
[12] R. Theissmann *et al.*, J. Appl. Phys. **102**, 024111 (2007).
[13] E. Aksel *et al.*, Appl. Phys. Lett. **98**, 152901 (2011).
[14] L. Jin, Z. B. He, and D. Damjanovic, Appl. Phys. Lett. **95**, 012905 (2009).
[15] D. A. Hall, Journal of Materials Science **36**, 4575 (2001).
[16] E. M. Bourim *et al.*, J. Appl. Phys. **91**, 6662 (2002).
[17] R. J. Harrison, S. A. T. Redfern, and E. K. H. Salje, Phys. Rev. B **69**, 144101 (2004).
[18] V. Mueller, Y. Shchur, and H. Beige, Ferroelectrics **269**, 201 (2002).
[19] A. A. Fedorenko, V. Mueller, and S. Stepanow, Phys. Rev. B **70** (2004).
[20] D. Damjanovic, Phys. Rev. B **55**, R649 (1997).
[21] D. Damjanovic, J. Appl. Phys. **82**, 1788 (1997).
[22] D. Damjanovic, in *The Science of Hysteresis*, edited by I. Mayergoyz, and G. Bertotti (Elsevier, 2005), pp. 337.
[23] J. L. Jones *et al.*, Appl. Phys. Lett. **89**, 092901 (2006).
[24] J. E. Daniels *et al.*, Appl. Phys. Lett. **95**, 032904 (2009).
[25] M. Davis, D. Damjanovic, and N. Setter, Phys. Rev. B **73**, 014115 (2006).
[26] W. W. Ge *et al.*, Physica Status Solidi-Rapid Research Letters **5**, 356 (2011).
[27] W. W. Ge *et al.*, Solid State Communications **151**, 71 (2011).
[28] M. Hinterstein *et al.*, Phys. Rev. Lett. **107** (2011).
[29] B. Kim *et al.*, J. Appl. Phys. **105**, 114101 (2009).
[30] X. L. Zhang *et al.*, Journal of Materials Science **18**, 968 (1983).
[31] D. Damjanovic, J. Am. Ceram. Soc. **88**, 2663 (2005).
[32] A. J. Studer, M. E. Hagen, and T. J. Noakes, Physica B-Condensed Matter **385-86**, 1013 (2006).
[33] J. Fried *et al.*, Nuclear Instruments & Methods in Physics Research Section A-Accelerators Spectrometers Detectors and Associated Equipment **478**, 415 (2002).
[34] J. A. Mead, and F. Bartsch, Ieee Nuclear Science Symposium Conference Record (2006).
[35] R. E. Eitel *et al.*, J. Appl. Phys. **96**, 2828 (2004).
[36] R. E. Eitel *et al.*, Japanese Journal of Applied Physics Part 1-Regular Papers Short Notes & Review Papers **41**, 2099 (2002).
[37] J. Rödel *et al.*, J. Am. Ceram. Soc. **92**, 1153 (2009).
[38] A. R. Damodaran *et al.*, Advanced Materials **23**, 3170 (2011).
[39] S. Bhattacharjee, and D. Pandey, J. Appl. Phys. **107** (2010).
[40] M. Ahart *et al.*, Nature **451**, 545 (2008).

[41] R. E. Eitel *et al.*, Japanese Journal of Applied Physics Part 1-Regular Papers Short Notes & Review Papers **41**, 2099 (2002).
[42] J. L. Jones, E. B. Slamovich, and K. J. Bowman, J. Appl. Phys. **97**, 034113 (2005).
[43] G. Tutuncu *et al.*, Phys. Rev. Lett. **108**, 177601 (2012).
[44] R. E. Eitel, T. R. Shrout, and C. A. Randall, J. Appl. Phys. **99**, 124110 (2006).
[45] J. E. Daniels, J. L. Jones, and T. R. Finlayson, Journal of Physics D, Applied Physics **39**, 5294 (2006).
[46] S. P. Li, W. W. Cao, and L. E. Cross, J. Appl. Phys. **69**, 7219 (1991).
[47] R. Tazaki *et al.*, Journal of Physics-Condensed Matter **21**, 215903 (2009).
[48] C. Moriyoshi *et al.*, Japanese Journal of Applied Physics **50**, 09NE05 (2011).
[49] D. A. Hall *et al.*, Acta Mater. **54**, 3075 (2006).
[50] V. Mueller, and Q. M. Zhang, Appl. Phys. Lett. **72**, 2692 (1998).
[51] D. V. Taylor, and D. Damjanovic, Appl. Phys. Lett. **73**, 2045 (1998).
[52] M. Davis *et al.*, J. Appl. Phys. **101**, 054112 (2007).
[53] S. J. Zhang, C. A. Randall, and T. R. Shrout, Appl. Phys. Lett. **83**, 3150 (2003).
[54] S. J. Zhang *et al.*, Journal of Crystal Growth **236**, 210 (2002).
[55] X. H. Du *et al.*, Appl. Phys. Lett. **72**, 2421 (1998).
[56] A. J. Bell, Journal of Materials Science **41**, 13 (2006).
[57] G. A. Rossetti, W. Zhang, and A. G. Khachaturyan, Appl. Phys. Lett. **88** (2006).
[58] A. J. Royles *et al.*, Appl. Phys. Lett. **98** (2011).
[59] J. Fu, R. Z. Zuo, and Z. K. Xu, Appl. Phys. Lett. **99** (2011).
[60] B. Peng, Z. X. Yue, and L. T. Li, J. Appl. Phys. **109** (2011).

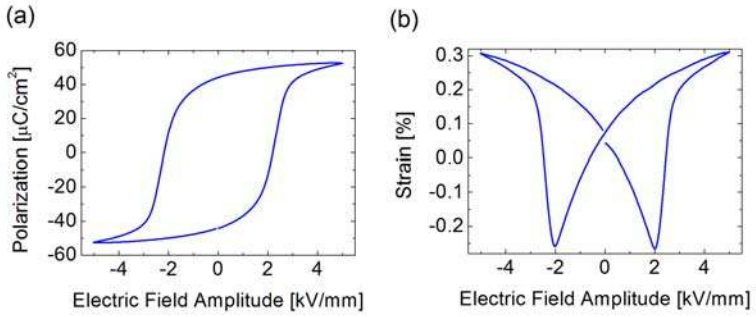

Figure 1. Polarization (a) and strain (b) as a function of electric field amplitude at high electric fields exceeding the ferroelectric coercive field.

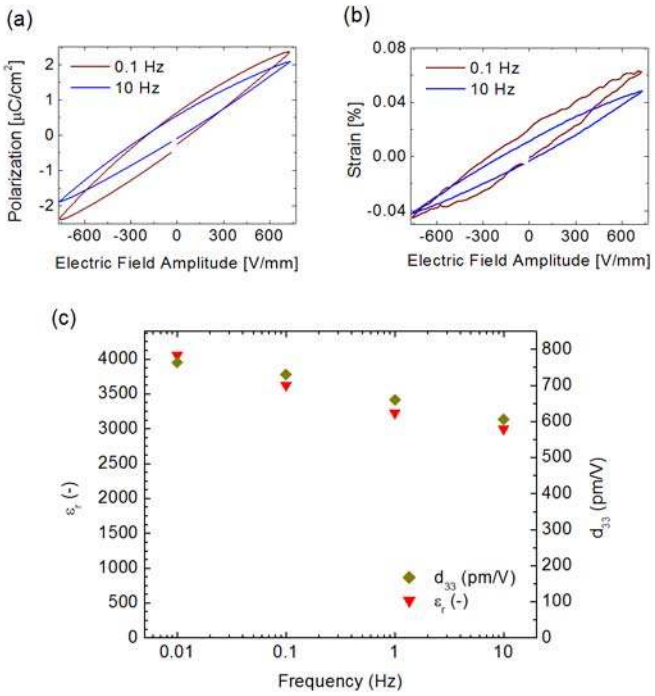

Figure 2. Representative polarization (a) and strain (b) measurements at subcoercive electric field amplitudes. A linear fit to the polarization and strain response yields the relative permittivity and longitudinal piezoelectric coefficients, shown in (c) as a function of frequency.

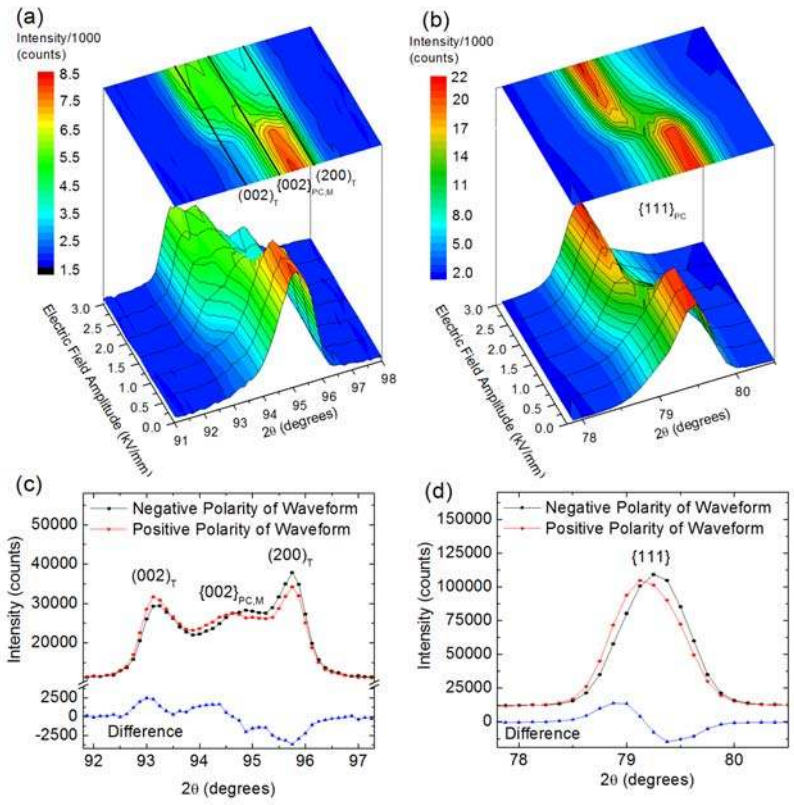

Figure 3. Diffraction patterns measured during static and dynamic electric field application. The diffraction patterns of the pseudo-cubic (a) {002} and (b) {111} regions as a function of applied electric field to an initially unpoled state. After poling, the (c) {002} and (d) {111} regions of the diffraction pattern during different polarities of an alternating, subcoercive electric field signal of frequency 1 Hz and ±0.75 kV/mm amplitude.

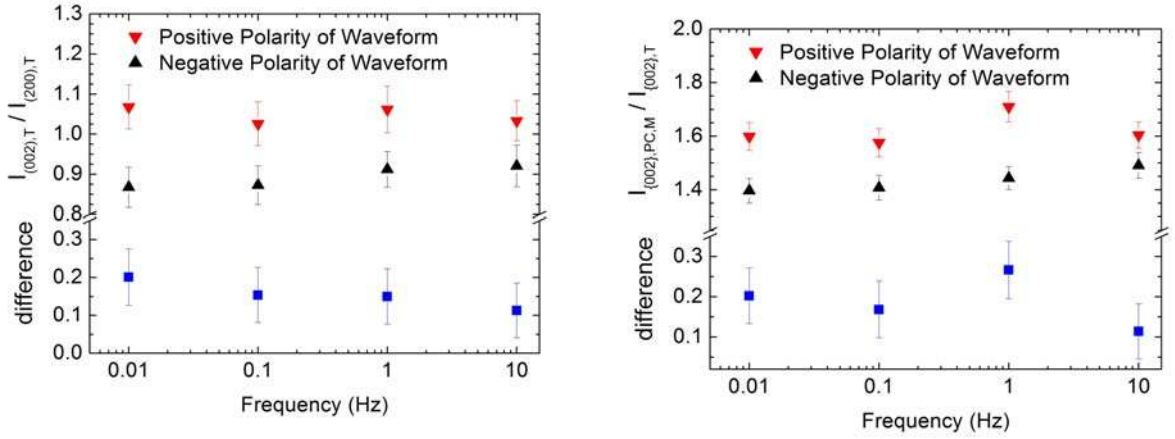

(a) (b)

Figure 4. Frequency and polarity dependence of diffraction intensity ratios. (a) Relative intensity of the tetragonal $(002)_T$ to $(200)_T$ reflections during the positive and negative polarities of an alternating electric field. (b) Relative intensity of the $\{002\}_{PC,M}$ profile to the total tetragonal intensity of the {002} reflections during the positive and negative polarities of the alternating electric field. The differences between these ratios are also shown. Error bars represent 68% confidence intervals from the profile fitting procedure.

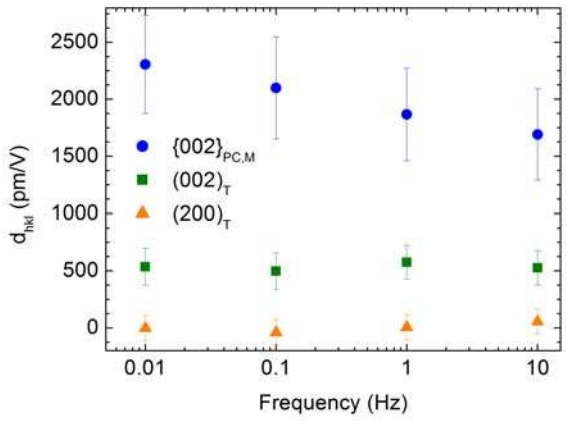

Figure 5. Frequency dependence of the electric-field-induced lattice strain coefficients. Electric-field-induced lattice strain coefficients are calculated as the lattice strain between the positive and negative polarities divided by the electric field amplitude. These results are shown for the tetragonal $(002)_T$ and $(200)_T$ and monoclinic $\{002\}_{PC,M}$ peaks as a function of frequency. Error bars represent 68% confidence intervals from the profile fitting procedure.

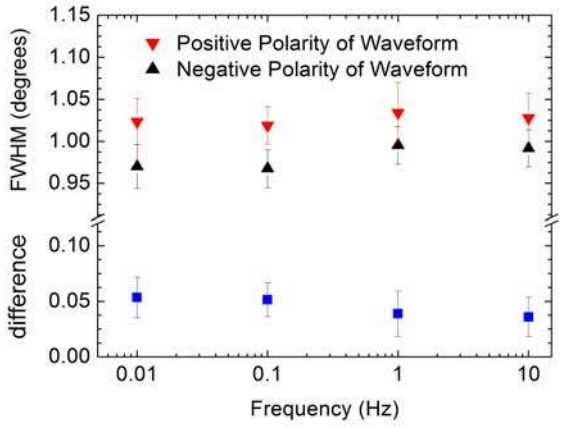

Figure 6. The frequency dependence of the full width at half maximum (FWHM) of the pseudo-cubic {111} profile is shown during the positive and negative polarities of the alternating electric field. The differences between these values are also shown. Error bars represent 68% confidence intervals from the profile fitting procedure.